J. Fluid Mech. (2013), *vol.* 731, *pp.* 117–141.
doi:10.1017/jfm.2013.372

Experiments on gravity currents propagating on different bottom slopes

Albert Dai†

Department of Water Resources and Environmental Engineering, Tamkang University, Taiwan 251-37, Taiwan

(Received 22 March 2013; revised 11 June 2013; accepted 15 July 2013; first published online 14 August 2013)

Experiments for gravity currents generated from an instantaneous buoyancy source propagating on an inclined boundary in the slope angle range $0^\circ \leqslant \theta \leqslant 9^\circ$ are reported. While the flow patterns for gravity currents on $\theta = 6^\circ, 9^\circ$ are qualitatively different from those on $\theta = 0^\circ$, similarities are observed in the acceleration phase for the flow patterns between $\theta = 2^\circ$ and $\theta = 6^\circ, 9^\circ$ and in the deceleration phase, the patterns for gravity currents on $\theta = 2^\circ$ are found similar to those on $\theta = 0^\circ$. Previously, it was known that the front location history in the deceleration phase obeys a power-relationship, which is essentially an asymptotic form of the solution to thermal theory. We showed that this power-relationship applies only in the early stage of the deceleration phase, and when gravity currents propagate into the later stage of the deceleration phase, viscous effects become more important and the front location data deviate from this relationship. When the power-relationship applies, it is found that at $\theta = 9^\circ$, $u_f(x_f + x_0)^{1/2}/B_0'^{1/2} \approx 2.88^{+0.19}_{-0.17}$, which changes to $2.86^{+0.13}_{-0.13}$ at $\theta = 6^\circ$, $2.54^{+0.08}_{-0.07}$ at $\theta = 2^\circ$, and $1.51^{+0.07}_{-0.07}$ on a horizontal boundary, where u_f is the front velocity, $(x_f + x_0)$ is the front location measured from the virtual origin, and B_0' is the released buoyancy. Our results indicate that in the slope angle range $6^\circ \leqslant \theta \leqslant 9^\circ$, the asymptotic relationship between the front velocity and front location in the deceleration phase is not sensitive to the variation of slope angle. In the late deceleration phase when the front location data deviate from the power-relationship, we found that the flow patterns for $\theta = 6^\circ, 9^\circ$ are dramatically different from those for $\theta = 0^\circ, 2^\circ$. For high slope angles, i.e. $\theta = 6^\circ, 9^\circ$, the edge of the gravity current head experiences a large upheaval and enrolment by ambient fluid towards the end of the deceleration phase, while for low slope angles, i.e. $\theta = 0^\circ, 2^\circ$, the gravity current head maintains a more streamlined shape without violent mixing with ambient fluid throughout the course of gravity current propagation. Our findings indicate two plausible routes to the finale of a gravity current event.

Key words: geophysical and geological flows, gravity currents

1. Introduction

Gravity currents, also known as buoyancy or density currents, are flows driven by a density difference mainly in the horizontal direction. The agents causing the density difference include temperature differentials, dissolved and suspended materials,

† Email address for correspondence: hdai@mail.tku.edu.tw

e.g. salt and sediments. Gravity currents produced by an instantaneous release of finite buoyancy source on a horizontal boundary, i.e. lock-exchange flows, have drawn much attention (see e.g. Shin, Dalziel & Linden 2004; Marino, Thomas & Linden 2005; Cantero *et al.* 2007; La Rocca *et al.* 2008, 2012*a*,*b*; Adduce, Sciortino & Proietti 2012). Gravity currents propagating down an inclined boundary have been considered less but are also commonly encountered in geophysical environments and engineering applications, such as powder-snow avalanches (Hopfinger 1983) and spillage of hazardous materials (Fannelop 1994). A comprehensive and informative review of the diversity of gravity currents is given in the monograph by Simpson (1997).

Categorized by the type of buoyancy source, gravity currents down an inclined boundary can be continuously supplied with buoyancy inflow (Britter & Linden 1980; Baines 2001, 2005) or they can be a surge-type flow generated by an instantaneous release of finite buoyancy (Beghin, Hopfinger & Britter 1981; Monaghan *et al.* 1999). The focus in this study is on the latter type of problem, i.e. gravity currents produced from a finite volume of heavy fluid down an inclined boundary, and to revisit the problem set forth in Beghin *et al.* (1981). In summary, their experiments show that, after the heavy fluid is released on a slope, the gravity currents first go through an acceleration phase followed by a deceleration phase. The thermal theory was developed therein to describe the front velocity history and has formed the basis for many subsequent studies, e.g. gravity currents with sediment resuspension from an erodable bed (Rastello & Hopfinger 2004) and with particle settling (Dade, Lister & Huppert 1994). Related to the present work, Webber, Jones & Martin (1993), Tickle (1996), and Ross, Linden & Dalziel (2002) used the shallow water model to consider a wedge-shaped cloud on a uniform slope. Birman *et al.* (2007) performed a two-dimensional numerical study of the full-depth lock-exchange problem on a slope, and Seon *et al.* (2007) performed gravity current experiments in tilted tubes, but the geometric configurations make their problems qualitatively different from that in Beghin *et al.* (1981).

Recently, Maxworthy & Nokes (2007) and Maxworthy (2010) conducted a series of experiments following Beghin *et al.* (1981), and reported their observations as follows. In the acceleration phase, the released heavy fluid continuously feeds the gravity current head with buoyancy from the following tail current like a line plume, and such flow patterns occur especially when the lock length is significantly greater than the lock height. In the deceleration phase, the gravity current head may lose buoyancy-containing fluid; nevertheless, in the whole range of the deceleration phase the front location data were reported to robustly follow the power-relationship, which is essentially an asymptotic form of the solution to thermal theory.

For the reader's convenience, the configuration of the problem set forth in Beghin *et al.* (1981) is sketched in figure 1 and the thermal theory with its variant forms is summarized as follows. Here the density of ambient fluid is taken as ρ_0 and the density of heavy fluid in the lock region is ρ_1, where we consider small density differences only, i.e. $\epsilon = (\rho_1 - \rho_0)/\rho_0 \ll 1$. The cross-sectional area of the lock region, which represents the total amount of released heavy fluid, is $A_0 = h_0 l_0$, where h_0 and l_0 are the lock height and lock length, respectively. After an instantaneous removal of the lock gate, the gravity current head develops a semi-elliptical shape, otherwise known as the 'thermal cloud', with the head height-to-head length ratio $k = H/L$.

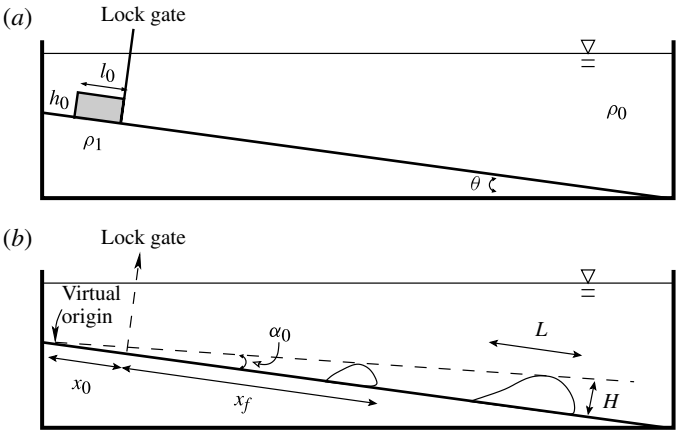

FIGURE 1. Side views of the channel used in the experiments for gravity currents produced from an instantaneous buoyancy source propagating on a slope which makes an angle θ with the horizontal. The ambient is filled with fluid of density ρ_0, and heavy fluid of density ρ_1 is confined in the lock region. H and L are the height and length of the gravity current head; x_0 is the distance between the virtual origin and the actual origin, i.e. the lock gate; x_f is measured from the gate to the gravity current front. In the initial state, the cross-sectional area of heavy fluid is $A_0 = h_0 l_0$ and the initial velocity is U_0, where $h_0 = 8$ cm and $l_0 = 10$ cm are the lock height and length, respectively.

The linear momentum equation with bottom friction term takes the form

$$\frac{\mathrm{d}(\rho + k_v \rho_0) S_1 HLU}{\mathrm{d}t} = B \sin\theta - C_f \rho U^2 L, \tag{1.1}$$

where ρ is the density of mixed fluid in the head, U is the mass-centre velocity of the head, t is the time, $k_v = 2k$ is the added mass coefficient (Batchelor 1967), $S_1 = \pi/4$ is a shape factor by which the cross-sectional area of the semi-elliptical head is defined as $S_1 HL$, θ is the slope angle, C_f is the friction coefficient on the bottom, which is approximately $C_f \approx 10^{-2}$ for a rough boundary and 2×10^{-3} for a saline cloud (Rastello & Hopfinger 2004), and $B = g(\rho - \rho_0) S_1 HL$ denotes the buoyancy that is contained in the head. Here we may assume that the gravity current head contains only a fraction χ of heavy fluid in the lock, i.e.

$$B = \chi \rho_0 \epsilon g A_0, \tag{1.2}$$

where $\chi = 1$ was assumed in Beghin *et al.* (1981) and $\chi < 1$ was reported in Maxworthy (2010). With turbulent entrainment assumptions (Ellison & Turner 1959), the mass conservation takes the form

$$\frac{\mathrm{d}}{\mathrm{d}t}(S_1 HL) = S_2 (HL)^{1/2} \alpha U, \tag{1.3}$$

where $S_2 = (\pi/2^{3/2})(4k^2 + 1)^{1/2}/k^{1/2}$ is another shape factor by which the circumference of the semi-elliptical head is defined as $S_2 (HL)^{1/2}$ and α is the entrainment coefficient.

With Boussinesq approximations, the front velocity of gravity current, u_f, follows the relation

$$u_f^2 = u_{f0}^2\left(\frac{x_{f0}}{x_f + x_0}\right)^{4+2C_f/(1+2k)\alpha_0 S_1} + \frac{2}{3 + 2C_f/(1+2k)\alpha_0 S_1} \times C\left(1 + \frac{\alpha_0}{2k}\right)^3 \frac{1}{x_f + x_0}\left[1 - \left(\frac{x_{f0}}{x_f + x_0}\right)^{3+2C_f/(1+2k)\alpha_0 S_1}\right], \tag{1.4}$$

where u_{f0} is the initial front velocity, x_{f0} is the distance from the 'virtual origin' to the initial front location, α_0 is the angle of growth, $C = 4kB\sin\theta/\pi(1+2k)\alpha_0^2\rho_0$, and x_0 is the distance from the 'virtual origin' to the lock gate. The reader is referred to appendix A for more details on the derivation.

If the gravity current starts with a quiescent initial condition, then the solution (1.4) can be further simplified when the gravity current is sufficiently far into the deceleration phase, i.e. when $(x_f + x_0)/x_{f0} \gg 1$,

$$u_f = \left[2/\left(3 + 2C_f/(1+2k)\alpha_0 S_1\right)\right]^{1/2} C^{1/2}(1 + \alpha_0/2k)^{3/2}(x_f + x_0)^{-1/2}. \tag{1.5}$$

Upon integration, (1.5) can be rewritten in the following form with an integration constant t_0:

$$(x_f + x_0)^{3/2} = K_M^{3/2} {B_0'}^{1/2}(t + t_0), \tag{1.6}$$

where $K_M = K_B\chi^{1/3}$ and $B_0' = \epsilon g A_0$. Note that K_B follows the form

$$K_B = \left(\frac{9}{6 + 4C_f/(1+2k)\alpha_0 S_1}\right)^{1/3}\left(\frac{4}{\pi}\right)^{1/3}(1 + \alpha_0/2k)\left[k\sin\theta/\alpha_0^2(1+2k)\right]^{1/3}. \tag{1.7}$$

Using the power-relationship (1.6), the front velocity in the deceleration phase follows

$$\frac{u_f(x_f + x_0)^{1/2}}{{B_0'}^{1/2}} = \frac{2}{3}{K_M}^{3/2}, \tag{1.8}$$

which is also the form for the front velocity in the deceleration phase given by Beghin *et al.* (1981), who reported that K_M varies approximately in the range between 2.35 and 2.60 at $\theta = 15°$ and reduces uniformly with increasing θ to a value between 1.56 and 1.87 at $\theta \approx 90°$.

It is worth noting that for gravity currents on a horizontal boundary, i.e. lock-exchange flows, the 'virtual origin' is taken at the lock gate and (1.8) reduces to

$$u_f = \tfrac{2}{3}{K_M}^{3/2}{B_0'}^{1/2}{x_f}^{-1/2}, \tag{1.9}$$

which is equivalent to the asymptotic behaviour of the front velocity in the inertial phase. Among other reports, $K_M = 1.6$ and 1.47 have been proposed by Hoult (1972) and Huppert & Simpson (1980), respectively, whereas Marino *et al.* (2005) suggest a range of 1.3–1.6 for full-depth releases and 1.4–1.8 for partial-depth releases. It is well known that the inertial phase is then followed by the viscous phase, in which the front velocity decays more rapidly than that in the inertial phase, i.e. $u_f \sim t^{-1/3}$. For example, Hoult (1972) derived $u_f \sim t^{-5/8}$ considering a balance between the viscous force from the interface and the buoyancy; the analysis was later revised by Huppert (1982), who accounted for the viscous effect over a rigid horizontal surface and reported that $u_f \sim t^{-4/5}$.

In this study, we re-investigated the propagation of planar gravity currents on inclined boundaries produced from an instantaneous buoyancy source. The primary objective is to observe the flow patterns as the gravity currents propagate down slopes and to identify how these patterns change with slope angles. With the experimental data, we may further validate the power-relationship for the front location histories in the deceleration phase and offer explanations for any discrepancy between the power-relationship and the front location data. Knowledge gained from this study will help shed light on the evolution of gravity currents on a slope in the deceleration phase and indicate plausible routes to the finale of a gravity current event.

2. Experiments

The channel used in the experiments was manufactured with a rectangular cross-section 0.2 m wide, 0.60 m deep and a length of 2.5 m with transparent Perspex sidewalls. A Perspex board, which is 2.47 m long and slightly less than 0.2 m wide, was placed in the channel as the inclined bottom slope, of which the angle can be adjusted in the range $0° \leqslant \theta \leqslant 9°$. The channel was reinforced by a specially designed steel cage. A sketch of the experimental set-up is shown in figure 1. The edges of the board were sealed with rubber sponge to prevent any leakage of fluid through the slits between the board and the sidewalls of the channel. During the experiments, the less dense fluid was fresh water and filled in the channel outside the lock region. The heavy fluid, a solution of sodium chloride, was injected into the lock mounted on the higher end of the inclined slope.

The lock was constructed with a height of 8 cm and a length of 10 cm and a gate which initially enclosed the heavy fluid in the lock. To allow injection of heavy fluid and escape of trapped air, two holes were drilled and tapped on the back of the lock. Removing the lock gate sets the heavy fluid into motion.

An electric light sheet and a light-diffusing screen were placed against the back wall. A Jai CVM 4 + CL CCD camera (1390 × 1024 pixel resolution at 24 frames per second) was positioned 6 m away from, and normal to, the front wall. The camera was also rotated at the same angle as the inclined board such that the x and y axes in the images align with the downslope and wall-normal directions. The heavy fluid in the lock was dyed with a trace of potassium permanganate to provide flow visualization. The dye absorbed the light along the path from the back to the front wall of the channel, and the attenuation of the light passing through the channel was measured and calibrated via the software DigiFlow (Dalziel 2012). Since potassium permanganate diffuses at approximately the same rate as sodium chloride, the dye concentration, c, can be used as a surrogate for the sodium chloride concentration and, therefore, the fluid density may be inferred (Shin *et al.* 2004; Marino *et al.* 2005; Nogueira *et al.* 2013), i.e. $\rho = \rho_0 + c(\rho_1 - \rho_0)$. Images of the gravity current were filmed at 24 frames per second and recorded directly onto a PC using the same software.

Densities were measured using a density meter with an accuracy of 10^{-4} g cm^{-3}. The kinematic viscosity of the sodium chloride solution is taken as $\nu = 1.1 \times 10^{-2}$ cm^2 s^{-1}. Densities of the heavy and light ambient fluids were around $\rho_1 \approx 1.0150$ g cm^{-3} and $\rho_0 \approx 0.9975$ g cm^{-3}, respectively, and the reduced gravity $g_0' = g(\rho_1 - \rho_0)/\rho_0$ was approximately $g_0' \approx 17.16$ cm s^{-2}. Density differences were chosen such that the gravity currents had Reynolds numbers based on the observed propagation speed and current thickness, in excess of 1000, above which viscous effects were previously thought to be unimportant (Simpson 1997). In all experiments,

Angle	g_0' (cm s^{-2})	t_{max} (s)	$x_{f\,max}$ (cm)	$u_{f\,max}$ (cm s^{-1})
$\theta = 9°$	$17.11^{+0.19}_{-0.19}$	$6.1^{+0.4}_{-1.1}$	$46.12^{+3.67}_{-10.07}$	$8.83^{+0.53}_{-0.44}$
$\theta = 6°$	$17.09^{+0.12}_{-0.08}$	$6.6^{+1.9}_{-0.6}$	$46.85^{+15.49}_{-5.93}$	$8.21^{+0.33}_{-0.24}$
$\theta = 2°$	$17.03^{+0.08}_{-0.12}$	$7.0^{+2.0}_{-1.5}$	$45.12^{+13.07}_{-11.82}$	$7.51^{+0.16}_{-0.17}$
$\theta = 0°$	$17.23^{+0.17}_{-0.21}$	$5.5^{+1.5}_{-1.0}$	$35.11^{+9.05}_{-6.19}$	$7.63^{+0.59}_{-0.45}$

TABLE 1. Table showing operational parameter, reduced gravity $g_0' = \epsilon g$, and the time, t_{max}, and front location, $x_{f\,max}$, at which the gravity current reaches its maximum front velocity, $u_{f\,max}$. Each value is the average of five experiments. The lock geometry, i.e. $h_0/l_0 = 8$ cm/10 cm, is maintained fixed for all experiments. The error estimates are to add and subtract the maximum and minimum values and are not the r.m.s. estimates.

the lock was submerged beneath the water surface by at least 10 cm to reduce the influence due to the free surface. From viewing the gravity current images, it is somewhat difficult to determine the rearward boundary of the head, since shedding of mixed fluid in the form of large, dyed vortices took place and the demarcation was hard to see. As done in previous studies, it is required to view the video in real time and make a subjective judgement of the length of the gravity current head.

3. Results

In what follows the experimental results for gravity currents produced from a buoyancy source of $h_0/l_0 = 8$ cm/10 cm on $\theta = 9°, 6°, 2°, 0°$ are presented in turn. Other operational parameters are listed in table 1. On each slope angle, at least five experiments were performed repeatedly to make qualitative and quantitative observations. The height and length of the lock, i.e. h_0 and l_0, remained fixed for all reported experiments. The Reynolds number in the experiments, i.e. $Re = \sqrt{\epsilon g h_0} h_0/\nu$ was approximately $Re \approx 8500$.

3.1. *Gravity currents on a $\theta = 9°$ slope*

3.1.1. *Qualitative features*

After removal of the lock gate, the heavy fluid was set into motion. Because the heavy fluid is released with a quiescent initial condition, the gravity current produced goes through an acceleration phase followed by a deceleration phase. Figure 2 presents the fluid concentration images for the gravity current on a 9° slope in the acceleration phase. The initial heavy fluid in the lock of dimensions $h_0/l_0 = 8$ cm/10 cm collapses with a small head forming at $t = 1.5$ s. As the collapse of heavy fluid continues, the height of heavy fluid in the lock region decreases and more heavy fluid is pushed into the head, as shown in figure 2 at $t = 2.5, 4.0$ s. As the gravity current further propagates in the acceleration phase, a semi-elliptical head forms, and outruns the tail current, as shown in figure 2 at $t = 5.5, 6.5$ s. We also note that a large roller consistently forms behind the head for the runs on a 9° slope, although the location of the roller may be slightly closer to or away from the head with some variability.

Figure 3 presents the concentration images for the gravity current on a 9° slope in the deceleration phase. As the gravity current propagates in this phase, the head maintains a semi-elliptical shape with persistent Kelvin–Helmholtz instabilities occurring on the upper edge of the gravity current head and with mixed fluid consistently left behind in the wake region, as shown in figure 3 at $t = 12, 18$ s.

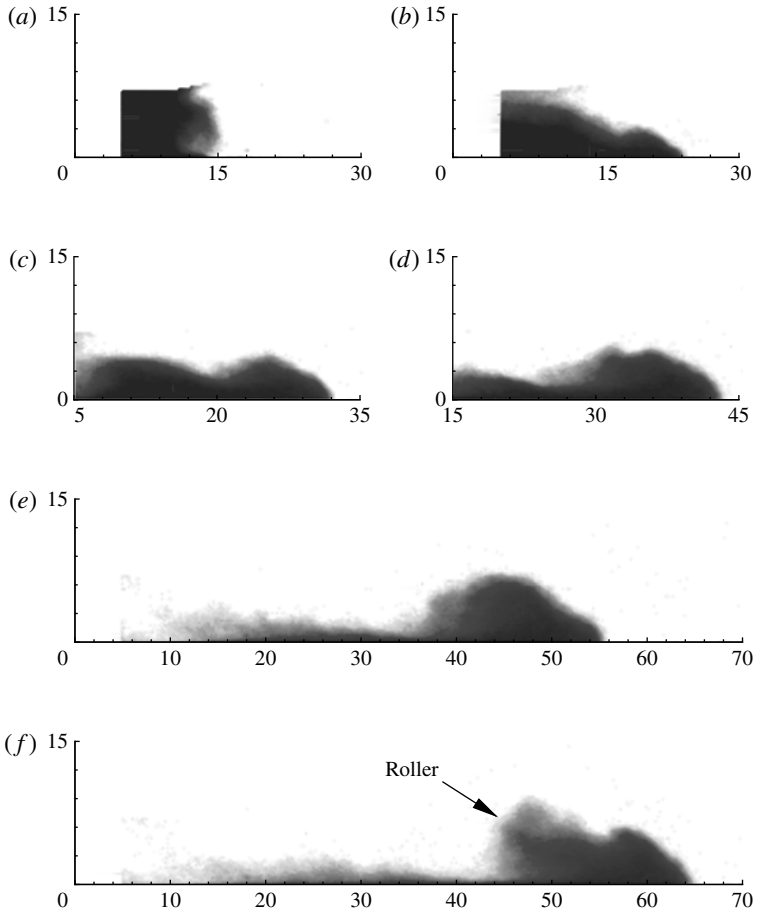

FIGURE 2. Experiment 10/03/12-1: fluid concentration images for the gravity current from a buoyancy source of $h_0/l_0 = 8$ cm/10 cm and $g'_0 = 17.11$ cm s^{-2} propagating on a 9° slope. Distances in the downslope and wall-normal directions are in units of cm. Time instances are chosen at (*a–f*) $t = 0$, 1.5, 2.5, 4.0, 5.5, 6.5 s in the acceleration phase.

What is surprising and reported here for the first time is that the gravity current on a 9° slope propagates with the described flow pattern in the deceleration phase for only a finite distance until a large upheaval of the interface between the head and ambient fluid takes place, as shown in figure 3 at $t = 28$ s. The uplifted mixed fluid is then quickly enrolled and engulfed by the ambient fluid. Once the large enrolment of mixed fluid and upheaval of the interface was initiated, the process was observed to occur repeatedly towards the end of the runs for gravity currents on a 9° slope.

3.1.2. *Quantitative results*

With the fluid concentration images in figures 2 and 3, the front location can be identified without ambiguity as the foremost part of the gravity current. After the front location is identified, the front velocity can be calculated as the time rate of change of the front location. Figure 4 shows the front location and front velocity histories for experiment 10/03/12-1. From the front velocity history, it is observed that the gravity current first goes through an acceleration phase followed by a deceleration

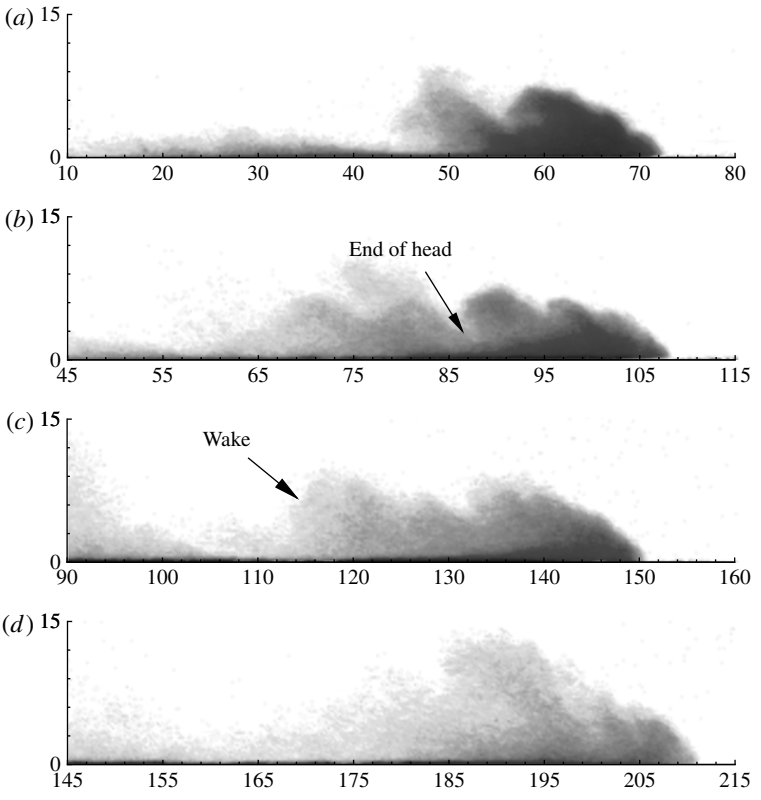

FIGURE 3. Experiment 10/03/12-1: fluid concentration images for the gravity current on a 9° slope. Distances in the downslope and wall-normal directions are in units of cm. Time instances are chosen at (*a–d*) $t = 7.5$, 12, 18, 28 s in the deceleration phase.

phase. At $t = 2.0$ s, the acceleration of the front begins to reduce significantly until $t = 6.5$ s, when the front velocity reaches its maximum value.

Figure 5 presents the $(x_f + x_0)^{3/2}$ versus t relationship for experiment 10/03/12-1. With the power-relationship (1.6), the deceleration phase is approximated by the solid straight line of best fit, of which the fitting equation is $(x_f + x_0)^{3/2} = 151.8(t + t_0)$, where $x_0 = 85.6$ cm and $t_0 = 3.7$ s. In figure 5, it is shown that the data approach the straight line from above, which is consistent with the experiments for gravity currents on $\theta = 10.6°$ and 5.9° reported by Maxworthy (2010). The data follow the straight line even at or before $t = 6.5$ s, when the gravity current reaches its maximum front velocity. The relationship is therefore shown to be robust in the deceleration phase. However, the front location of the gravity current follows the power-relationship in the deceleration phase for only a finite distance. Starting at $t \approx 24$ s, the data start to deviate from and fall below the fitting straight line, as shown in figure 5 and the inset close-up view for $t \geqslant 20$ s. The departure from the power-relationship is consistently observed for the runs of gravity currents on the 9° slope and such departure indicates that the front velocity decays more rapidly. It should be noted that it is at this stage of motion that the large upheaval of the interface of the gravity current head and the engulfment of uplifted mixed fluid by ambient fluid begin, as shown by the flow pattern at $t = 28$ s in figure 3. Values of the head Reynolds numbers,

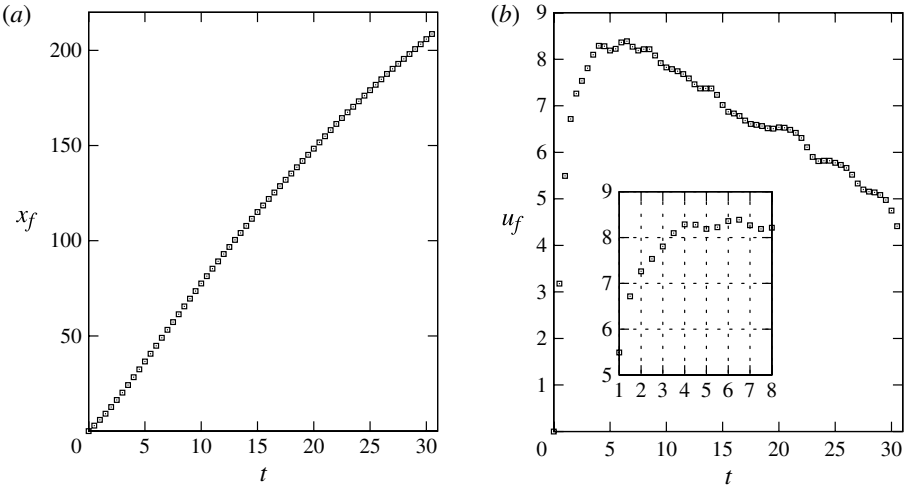

FIGURE 4. Experiment 10/03/12-1: front location and front velocity against time for the gravity current produced from a buoyancy source of $h_0/l_0 = 8\,\text{cm}/10\,\text{cm}$ and $g'_0 = 17.11\,\text{cm}\,\text{s}^{-2}$ on a 9° slope. The front location is measured from the lock gate. The front location is in units of cm, time is in s, and the front velocity is in cm s^{-1}.

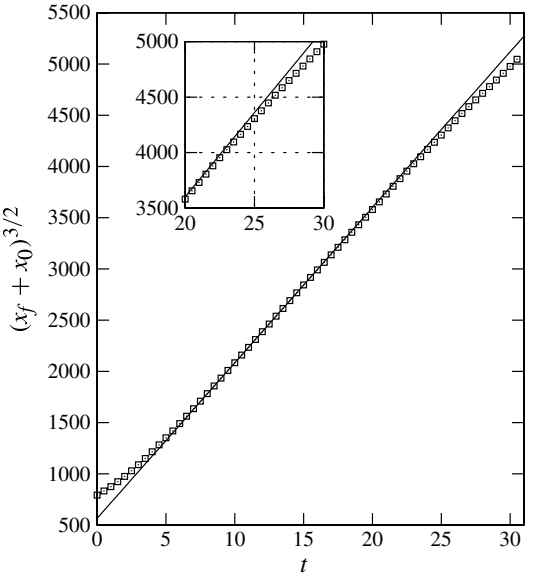

FIGURE 5. Experiment 10/03/12-1: $(x_f + x_0)^{3/2}$ versus t for the gravity current on a 9° slope. The front location is in units of cm and time is in s. The solid line represents the straight line of best fit to the deceleration phase and the fitting equation is $(x_f + x_0)^{3/2} = 151.8(t + t_0)$, where $x_0 = 85.6$ cm and $t_0 = 3.7$ s. In this case the maximum front velocity $u_f = 8.39\,\text{cm}\,\text{s}^{-1}$ occurs at $t \approx 6.5$ s and $x_f \approx 49$ cm.

i.e. $Re_H = u_f H/\nu$, were estimated in the range $2500 \lesssim Re_H \lesssim 3500$ for the runs when the departure of data from the power-relationship is observed. Additional runs for gravity currents on slopes with higher Reynolds numbers, $Re \approx 14\,000, 20\,000, 26\,000,$

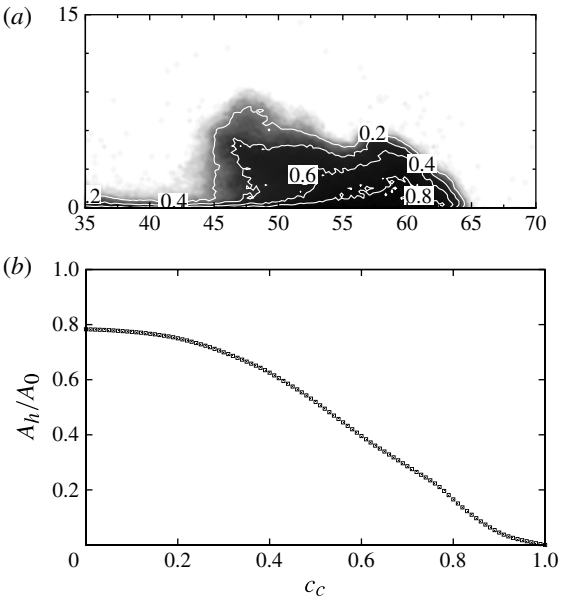

FIGURE 6. Experiment 10/03/12-1. (*a*) Close-up view of the head region of the gravity current on a 9° slope at $t = 6.5$ s, where the distances in the downslope and wall-normal directions are in units of cm. White solid lines represent the concentration contours and the numbers indicate the concentration values. (*b*) Ratio of buoyancy contained within the head region to the total released buoyancy for the gravity current on a 9° slope at $t = 6.5$ s. A_h/A_0 is defined according to (3.1) and A_h represents the buoyancy within the head region of which the width-averaged concentration exceeds c_c.

were also performed and the head Reynolds numbers were estimated in a consistent range as the front location data deviate from the power-relationship. In previous works, viscous effects were thought to be unimportant for Reynolds numbers in this range and the gravity currents were expected to propagate in the whole range of the deceleration phase following the power-relationship (1.6). However, our scaling analysis (appendix B) shows that it is possible that for gravity currents at this stage of motion in the deceleration phase, the Reynolds number is low enough that viscous effects could be unexpectedly more important.

Figure 6(*a*) shows the close-up view for the head region of the gravity current on a 9° slope at $t = 6.5$ s. The concentration contours are plotted with concentration values for reference. With the concentration contours, the density distribution inside the gravity current head is now revealed. Towards the front part of the head the density gradient across the interface is steep compared with that in the wake region on the back of the head. Part of the heavy fluid in the head remains almost unmixed in the core of the head region, e.g. $c > 0.8$, when the gravity current reaches the maximum front velocity. To calculate the amount of heavy fluid in the lock that is actually contained within the head region when the maximum front velocity is reached, the fluid concentration in the head region is integrated according to

$$\frac{A_h}{A_0} = \int_{x_f - L}^{x_f} \int_0^{\infty} c(x, y)|_{c \geqslant c_c} \, \mathrm{d}y \, \mathrm{d}x, \tag{3.1}$$

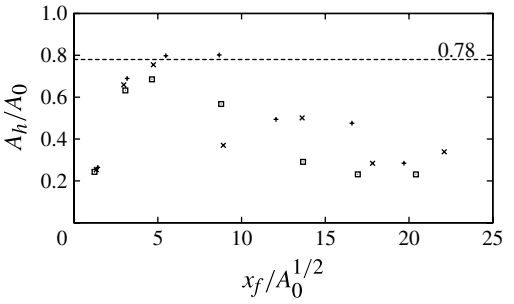

FIGURE 7. Ratio of buoyancy contained within the head to the total released buoyancy versus the front location normalized by $A_0^{1/2}$. The buoyancy ratio in the head region is evaluated using (3.1) with $c_c = 10^{-2}$. Symbols: +, experiment 10/03/12-1 for the gravity current on $\theta = 9°$; ×, experiment 10/08/12-3 for the gravity current on $\theta = 6°$; ⊡, experiment 10/10/12-5 for the gravity current on $\theta = 2°$. The dashed line represents $A_h/A_0 = 0.78$, which is estimated for $\theta = 9°$ via $\chi = [K_M/K_B]^3$ using measured parameters.

where A_h is the amount of heavy fluid contained within the head region of which the width-averaged concentration exceeds c_c, and x and y are the coordinates in the streamwise and wall-normal directions, respectively. The length of the head, L, in (3.1) is not a predetermined constant but a variable distance between the front location and the end of the head, which requires us to view the concentration images in real time and to use subjective judgement to determine the end of the head. For example, in figure 3 at $t = 12$ s, the end of the head is indicated by an arrowhead. Figure 6(*b*) shows the ratio of heavy fluid in the head region, of which the concentration value exceeds c_c, to the total released heavy fluid against the threshold value c_c. It should be noted that the contour defined by the threshold value c_c also draws a boundary for the core region of the head. Obviously, the core region defined by a higher value of c_c is more compact in size and shape. Using the threshold value c_c allows us to estimate the amount of heavy fluid inside the core region. For example, it is observed that 75 % of the released heavy fluid in the head region is bounded by $c_c = 0.2$ at $t = 6.5$ s. Instead, as the boundary is taken as $c_c = 0.6$, it is estimated that only 40 % of the released heavy fluid is contained in the core region of the head.

Using the power-relationship, it is possible to theoretically estimate the amount of heavy fluid contained within the head as the gravity current propagates into the deceleration phase. With the fitting equation $(x_f + x_0)^{3/2} = 151.8(t + t_0)$, where ${K_M}^{3/2}{B_0'}^{1/2} = 151.8$ cm$^{3/2}$ s^{-1}, the fraction $\chi = 0.78$ can be calculated via $\chi = [K_M/K_B]^3$ using the measured parameters $k = 0.3$ and $\alpha_0 = 0.0538$, as listed in table 2. From figure 7 it is shown that the power-relationship not only robustly describes the front location data in the early stage of the deceleration phase but also provides a reasonably good estimate for the amount of heavy fluid contained within the head, even though the gravity current head may lose buoyancy as it propagates. In the deceleration phase, mixed fluid is shed from the head and left behind in the wake region, the buoyancy contained within the head may gradually decrease. Towards the end of the deceleration phase, mixed fluid in the head is uplifted and engulfed by the ambient fluid. Therefore, the buoyancy in the head, i.e. the downslope driving force, is significantly reduced, which is also an important factor for the front location data falling below the power-relationship represented by the straight fitting line.

Angle	k	α_0	$x_0/{A_0}^{1/2}$	$t_0{g_0'}^{1/2}/{A_0}^{1/4}$	K_M	K_B	χ
$\theta = 9°$	$0.26^{+0.036}_{-0.048}$	$0.0549^{+0.0020}_{-0.0015}$	$9.19^{+0.77}_{-0.60}$	$17.00^{+1.53}_{-1.21}$	$2.64^{+0.08}_{-0.08}$	$2.82^{+0.08}_{-0.12}$	$0.82^{+0.16}_{-0.14}$
$\theta = 6°$	$0.24^{+0.025}_{-0.012}$	$0.0409^{+0.0008}_{-0.0007}$	$14.01^{+0.97}_{-0.54}$	$25.91^{+1.81}_{-0.98}$	$2.64^{+0.13}_{-0.09}$	$2.91^{+0.09}_{-0.06}$	$0.75^{+0.12}_{-0.14}$
$\theta = 2°$	$0.20^{+0.023}_{-0.021}$	$0.0254^{+0.0049}_{-0.0026}$	$17.80^{+1.38}_{-1.66}$	$32.85^{+2.63}_{-2.00}$	$2.43^{+0.06}_{-0.04}$	$2.64^{+0.06}_{-0.07}$	$0.78^{+0.03}_{-0.04}$
$\theta = 0°$	—	—	—	—	$1.72^{+0.06}_{-0.11}$	0	—

TABLE 2. Table showing dependent variables and the estimated effective buoyancy ratio, χ, in the deceleration phase. Each value is the average of five experiments. The lock geometry, i.e. $h_0/l_0 = 8$ cm/10 cm, is maintained fixed for all experiments. The error estimates are to add and subtract the maximum and minimum values and are not the r.m.s. estimates.

Using the power-relationship fitting equation, we derive that the front velocity follows $u_f(x_f + x_0)^{1/2}/{B'_0}^{1/2} \approx 2.88^{+0.19}_{-0.17}$ in the deceleration phase, which is consistent with $u_f(x_f + x_0)^{1/2}/{B'_0}^{1/2} \approx 2.6 \pm 0.2$ for gravity currents on $\theta = 15°$ as reported by Beghin *et al.* (1981).

3.2. *Gravity currents on a $\theta = 6°$ slope*

The gravity current on a 6° slope is qualitatively similar to that on a 9° slope in both the acceleration and deceleration phases. As reported previously, here the gravity current head maintains a semi-elliptical shape with an identifiable wake region, as shown in figure 8. But we note that the size of roller behind the head is reduced, as shown in figure 8 at $t = 6.0$ s. It is worth pointing out that towards the end of the deceleration phase the large upheaval of the interface between the head and ambient fluid followed by engulfment of uplifted mixed fluid by ambient fluid, as was observed for gravity currents on a 9° slope, is still present here on a 6° slope, as shown in figure 8 at $t = 31.5$ s.

Figure 9 shows the front velocity and $(x_f + x_0)^{3/2}$ against time for the gravity current on a 6° slope. The power-relationship is robust in the deceleration phase during 6.0 s $\lesssim t \lesssim$ 22.5 s. With the large upheaval of the interface occurring repeatedly towards the end of the deceleration phase as shown in figure 8 at $t = 31.5$ s, it is not a surprise to observe the deviation of the front location data from the power-relationship, as discussed in the previous section for the gravity current on a 9° slope. At this stage, the head Reynolds numbers were estimated in the range $2000 \lesssim Re_H \lesssim 3000$.

For gravity currents on a 6° slope, the fraction of heavy fluid in the lock that is contained within the head is estimated as $\chi = 0.75^{+0.12}_{-0.14}$ via $\chi = [K_M/K_B]^3$, which appears to be slightly lower than the fraction for gravity currents on a 9° slope and is also consistent with our findings from the experiments, as shown in figure 7. From table 2, it is observed that K_M for $\theta = 6°$ varies in approximately the same range overlapping with that for $\theta = 9°$. It is worth noting that in the experiments for gravity currents on $\theta = 5.9°, 10.6°$ reported by Maxworthy (2010), K_M varied erratically from 2.5 to 2.9 without distinguishable dependence of K_M on slope angle. Nor can we identify the relationship between K_M and θ here merely based on the results for $\theta = 6°, 9°$. According to Beghin *et al.* (1981) and using (1.8), K_M is found to increase from 2.0 at $\theta = 5°$ to its maximum value 2.5 ± 0.1 at $\theta = 15°$ and decrease uniformly to 1.7 ± 0.2 at $\theta \approx 90°$. It is very likely that, albeit with some scatter in data, K_M assumes its maximum value in the slope angle range $6° \lesssim \theta \lesssim 10°$ as studied here and in Maxworthy (2010). As a result, no clear dependence of K_M on θ could be identified in this slope angle range.

3.3. *Gravity currents on a $\theta = 2°$ slope*

For gravity currents on a 2° slope, similarities with the flow patterns of gravity currents on $\theta = 6°$ and 9° in the acceleration phase are found but a number of qualitative differences in the flow patterns are observed in the deceleration phase. The heavy fluid in the lock collapses and pushes out a head as reported previously, but the large roller behind the head no longer exists when the gravity current reaches its maximum front velocity, as shown in figure 10 at $t = 6.5$ s. The gravity current head still maintains a 'cloud' form which is separate from the tail current, but the shape of the head is now more streamlined compared with those on the 6° and 9° slopes. When the gravity current propagates into the deceleration phase on a 2° slope, the wake region with intense mixing is observed for a limited duration of time, as shown in figure 10 at $t = 12.5$ s. As the gravity current moves further into the deceleration

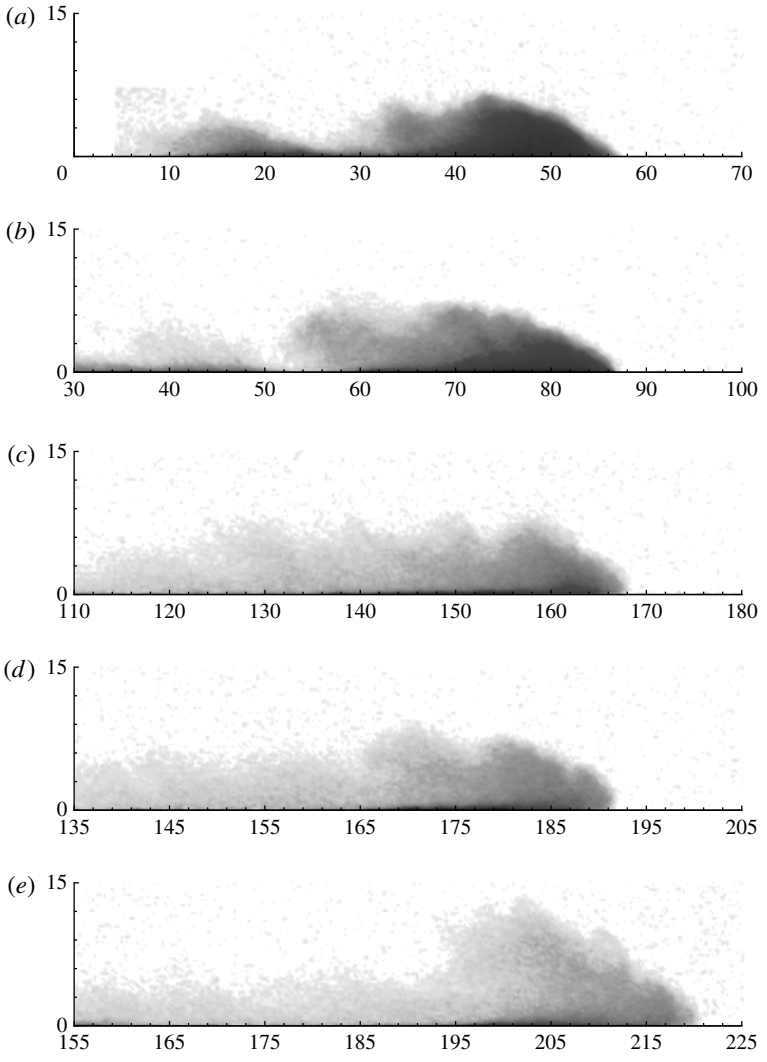

FIGURE 8. Experiment 10/08/12-3: fluid concentration images for the gravity current from a buoyancy source of $h_0/l_0 = 8$ cm/10 cm and $g_0' = 17.11$ cm s^{-2} propagating on a 6° slope. Distances in the downslope and wall-normal directions are in units of cm. Time instances are chosen at (*a–e*) $t = 6.0, 10, 22, 26, 31.5$ s when the maximum front velocity is reached at $t = 6$ s and in the deceleration phase.

phase, the demarcation between the head and the tail current becomes less clear. Instead of intense mixing with ambient fluid and travelling individually as a 'cloud' entity, the gravity current at this stage in the deceleration phase tends to behave more like 'spreading' on the slope, as shown in figure 10 at $t = 20, 36$ s. It is worth noting that the large upheaval of the interface is no longer observed here towards the end of the deceleration phase, as reported previously for $\theta = 6°, 9°$. The gravity current head maintains a more streamlined shape throughout its course of motion.

Figure 11 shows the front velocity and $(x_f + x_0)^{3/2}$ against time for the gravity current on a 2° slope. As in $\theta = 6°, 9°$, the gravity current goes through an

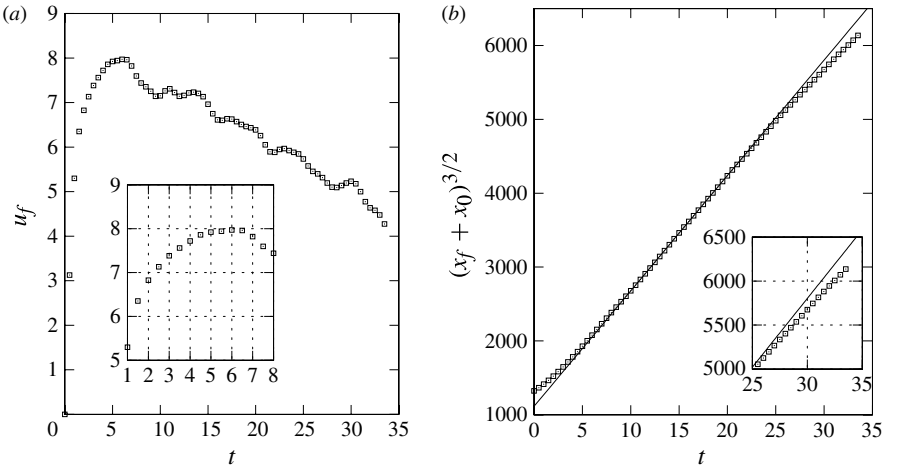

FIGURE 9. Experiment 10/08/12-3: front velocity versus time for the gravity current produced from $h_0/l_0 = 8$ cm/10 cm and $g_0' = 17.11$ cm s^{-2} on a 6° slope. The front velocity is in units of cm s^{-1}, the front location is in cm, and time is in s.

acceleration phase followed by a deceleration phase. While the approach to the straight fitting line is from above in $\theta = 6°, 9°$, the approach to the straight fitting line in $\theta = 2°$ is from below, which is typical of experiments with sufficiently low driving force, e.g. small slope angle in this case. As in previous cases, the power-relationship is robust only in the early deceleration phase, e.g. $8.5 \lesssim t \lesssim 23.5$ s in figure 11. When the gravity current propagates further into the deceleration phase, the data begin to fall below the straight fitting line as $t \gtrsim 23.5$ s. While viscous effects are considered more important in the deceleration phase when the front location data fall below the power-relationship, the flow pattern on the 2° slope at this stage of motion is very different from those on $\theta = 6°, 9°$. What is different from the results observed on 6° and 9° slopes is that the large upheaval of the interface and the engulfment of uplifted mixed fluid by ambient fluid as the front location data deviate from the power-relationship are not observed, and the head maintains a more streamlined shape, with a tail current tapering off towards the end of the deceleration phase.

Using the power-relationship, we may estimate the fraction of heavy fluid in the lock that is contained within the head to be $\chi = 0.78^{+0.03}_{-0.04}$ and the experimental constant $K_M = 2.43^{+0.06}_{-0.04}$. We should note that K_M takes a value obviously smaller than those for $\theta = 6°, 9°$. This observation confirms the notion that in the slope angle range $6° \lesssim \theta \lesssim 10°$, K_M would very likely assume its maximum value. The dependence of K_M on θ becomes apparent as the slope angle is sufficiently away from this range, i.e. that K_M decreases as θ decreases below this slope angle range $6° \lesssim \theta \lesssim 10°$.

3.4. *Gravity currents on a $\theta = 0°$ slope*

The concentration images for the gravity current on a horizontal boundary is shown in figure 12. In the experiments for $\theta = 0°$, the lock was submerged beneath the water surface by at least 40 cm. This case is also known as the partial-depth lock-exchange flow and the lock height to ambient water depth ratio is below 0.2. It has been reported that in this case the front velocity goes through a slumping phase followed by an inertial phase and then a viscous phase, while the gravity currents decelerate in

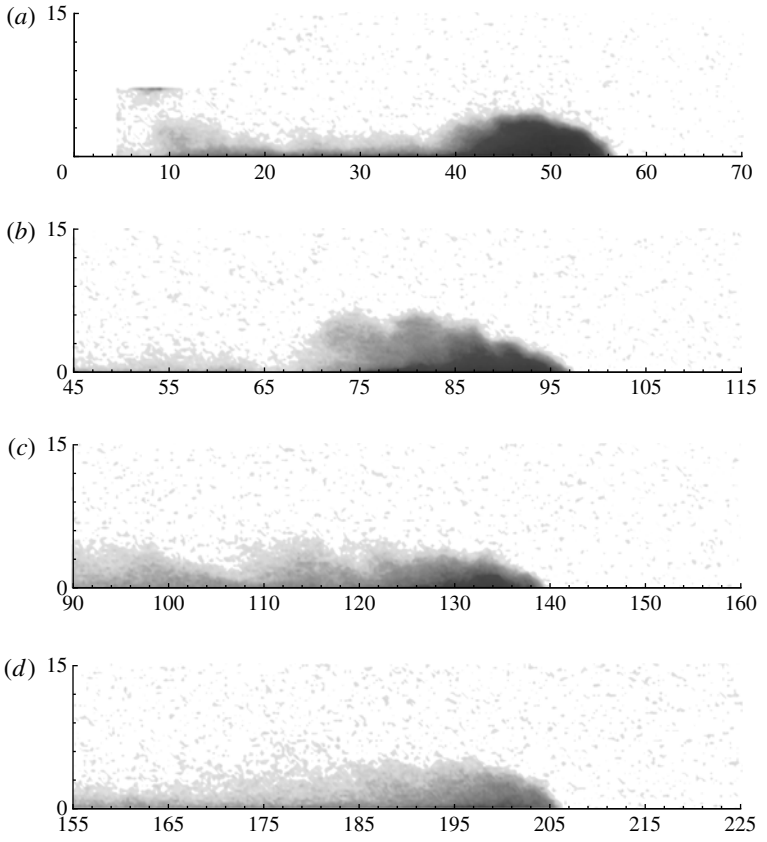

FIGURE 10. Experiment 10/10/12-5: fluid concentration images for the gravity current from a buoyancy source of $h_0/l_0 = 8$ cm/10 cm and $g_0' = 17.02$ cm s^{-2} propagating on a 2° slope. Distances in the downslope and wall-normal directions are in units of cm. Time instances are chosen at (*a–d*) $t = 6.5$, 12.5, 20, 36 s. In this case the maximum velocity occurs at $t \approx 6.5$ s.

both the inertial and viscous phases. In the inertial phase, the front velocity follows the asymptote $\tilde{u}_f \sim \tilde{t}^{-1/3}$, while in the viscous phase, $\tilde{u}_f \sim \tilde{t}^{-5/8}$ and $\tilde{u}_f \sim \tilde{t}^{-4/5}$ were reported by Hoult (1972) and Huppert (1982), respectively, where the dimensionless front velocity is $\tilde{u}_f = u_f/\sqrt{g_0' h_0}$ and the dimensionless time is $\tilde{t} = t\sqrt{g_0' h_0}/l_0$. As shown in figure 13, the inertial and viscous phases are both identifiable in experiment 10/10/12-3 for the gravity current on $\theta = 0°$. The gravity current is in the inertial phase during $9 \lesssim \tilde{t} \lesssim 21$, i.e. $8 \lesssim t \lesssim 18$ s in dimensional time, and then moves into the viscous phase when $\tilde{t} \gtrsim 21$, i.e. $t \gtrsim 18$ s.

From the concentration images, we find that a gravity current head quickly forms as the heavy fluid is released from the lock, but the mixing with ambient fluid is not as violent as in the gravity currents on $\theta = 6°, 9°$. The head does not overrun the tail current throughout the motion and the gravity current appears more like 'spreading' on the boundary, as observed for the gravity current on $\theta = 2°$ in the deceleration phase.

For gravity currents on a horizontal boundary, the height of the head does not increase as in other cases for $\theta = 2°, 6°, 10°$. Therefore, extrapolation of head height to identify the virtual origin is not applicable. But still we may follow Beghin *et al.* (1981) and the front location data could be recast in the power-relationship

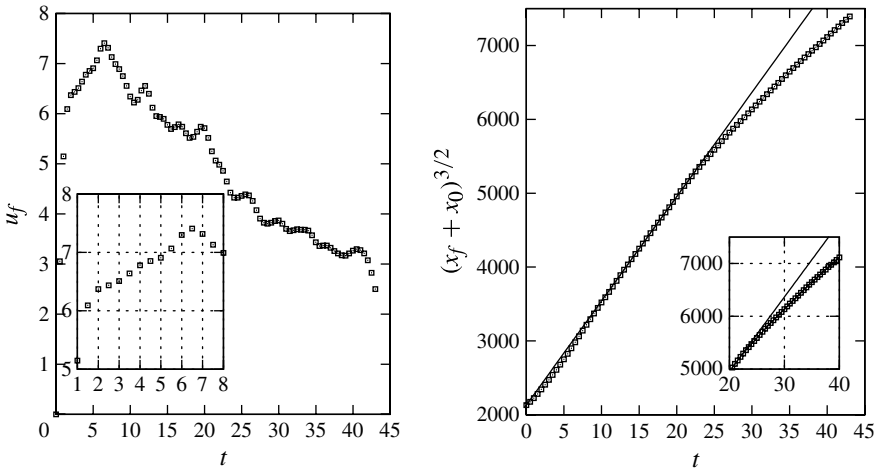

FIGURE 11. Experiment 10/10/12-5: front velocity and $(x_f + x_0)^{3/2}$ versus time for the gravity current produced from a buoyancy source of $h_0/l_0 = 8\,\text{cm}/10\,\text{cm}$ and $g_0' = 17.02\,\text{cm}\,\text{s}^{-2}$ on a 2° slope. The front velocity is in units of $\text{cm}\,\text{s}^{-1}$, the front location is in cm, and time is in s.

form, where the front location is now measured from the lock gate, i.e. $x_0 = 0$ cm, rather than from the virtual origin. Figure 14 shows ${x_f}^{3/2}$ against time for experiment 10/10/12-3. It is seen that when the gravity current decelerates, the power-relationship consistently applies in the whole range of the inertial phase and in the early viscous phase, i.e. $8 \lesssim t \lesssim 21$ s; but when the viscous effects dominate, the front location data begin to fall off from the straight fitting line, as shown in figure 14 at $t \gtrsim 21$ s.

It is worth noting that in the viscous phase, the gravity current extends on the horizontal boundary with the tail current persistently joining the head throughout the course of motion. The observation for the flow patterns for gravity currents on a horizontal boundary when the gravity currents decelerate is qualitatively similar to that on $\theta = 2°$ in the deceleration phase, where the large upheaval of the interface in $\theta = 6°, 9°$ is not present and the gravity current maintains a more streamlined head with a connecting tail current.

Although $K_B = 0$ for $\theta = 0°$ may prohibit us from estimating the parameter χ via $\chi = [K_M/K_B]^3$, still K_M can be derived with the power-relationship (1.6) when applied in the inertial and early viscous phases. As listed in table 2, $K_M = 1.72^{+0.06}_{-0.11}$ is derived using the data collected in this study. It should be noted that for planar gravity currents on a horizontal boundary, $K_M = 1.6$ and 1.47 have been proposed by Hoult (1972) and Huppert & Simpson (1980), respectively, while in a more recent study, Marino *et al.* (2005) suggests a range for K_M between 1.4 and 1.8 for partial-depth lock-exchange flows. Our findings of K_M for gravity currents on a horizontal boundary appear to be in excellent agreement with reported values. In addition, K_M reported here for $\theta = 0°$ is less than those for $\theta = 2°, 6°, 9°$, as we expected and discussed in the above sections.

4. Discussions

Gravity currents produced from an instantaneous buoyancy source propagating on an inclined boundary in the slope angle range $0° \leqslant \theta \leqslant 9°$ are presented here. The main

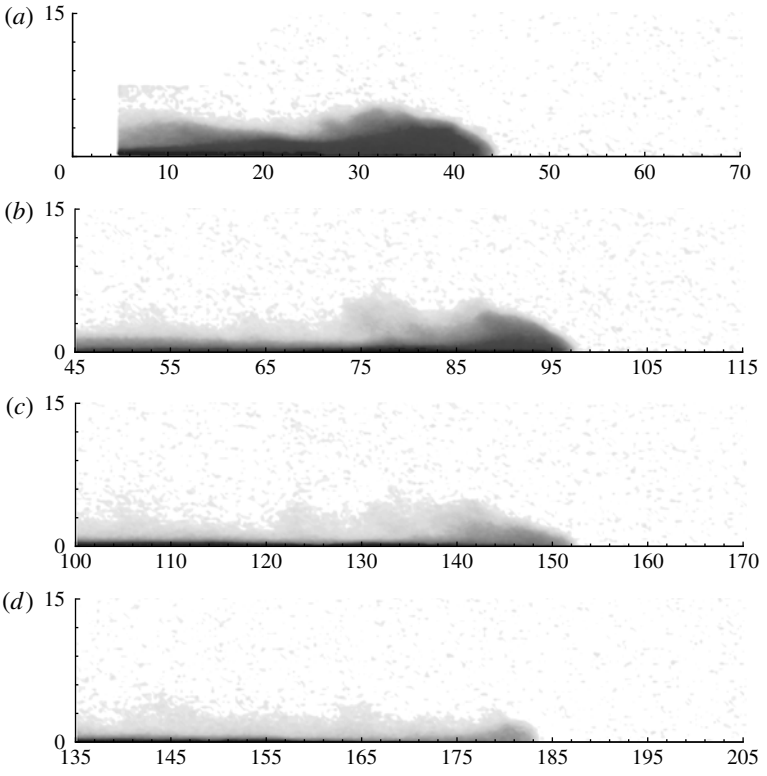

FIGURE 12. Experiment 10/10/12-3: fluid density images for the gravity current on a 0° slope. Distances in the downslope and wall-normal directions are in units of cm. Time instances are chosen at (*a–d*) $t = 4.5, 12, 22, 30$ s. In this case the maximum velocity occurs at $t \approx 4.5$ s and the gravity current is in the inertial phase at $t \approx 12$ s and in the viscous phase at $t \approx 30$ s.

discussion concerns the applicability of the power-relationship for the front location history in the deceleration phase and the flow patterns observed when the data deviate from this relationship. It was reported in previous studies that the power-relationship was robust in the whole range of the deceleration phase, but we showed that it may not be so. The front location data for gravity currents on $\theta = 6°, 9°$ follow the power-relationship only in part of the deceleration phase. When the front location data fall below this relationship at the later stage of the deceleration phase, large upheaval of the interface between the head and ambient fluid and engulfment of uplifted mixed fluid by ambient fluid are repeatedly observed towards the end of the deceleration phase. Similarly, for gravity currents on $\theta = 0°, 2°$, the front location data follow the power-relationship in only part of the deceleration phase and fall below this relationship when viscous effects are important. However, contrary to the flow patterns for gravity currents on $\theta = 6°, 9°$, the head maintains a streamlined shape without violent mixing towards the end of the deceleration phase. Our findings here indicate two plausible routes, namely on high and low slope angles, to the finale of a gravity current event when the agents causing the density difference, e.g. salinity, sediments, or particles, do not settle out from the gravity current or when the fall velocity of the particles is sufficiently small.

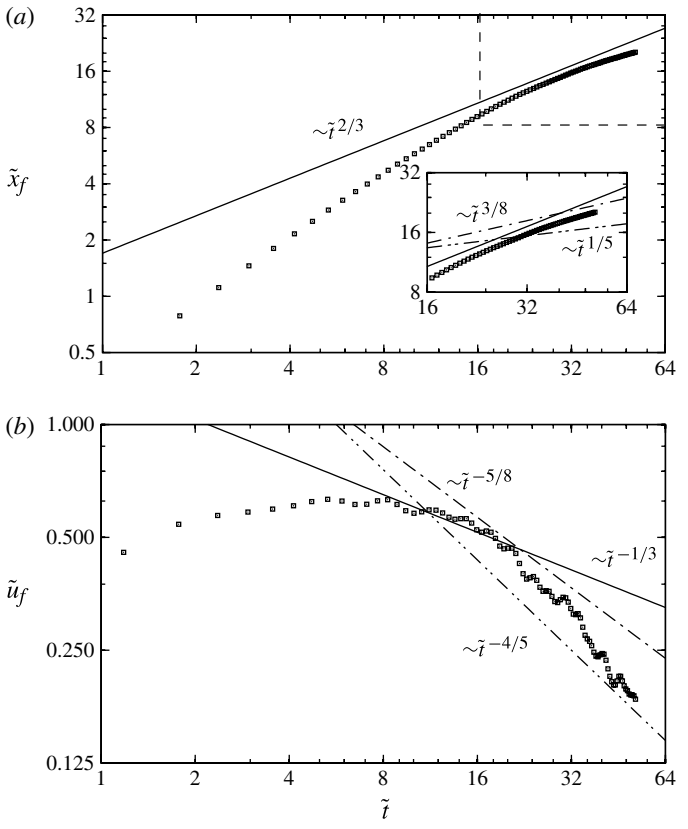

FIGURE 13. Experiment 10/10/12-3: (*a*) front location versus time and (*b*) front velocity versus time, for the gravity current produced from $h_0/l_0 = 8$ cm/10 cm and $g_0' = 17.40$ cm s^{-2} on a 0° slope. The inset figure in (*a*) shows the close-up view for $16 \leqslant \tilde{t} \leqslant 64$. The dimensionless front location is defined as $\tilde{x}_f = x_f/l_0$, the dimensionless front velocity is $\tilde{u}_f = u_f/\sqrt{g_0' h_0}$, and dimensionless time is $\tilde{t} = t\sqrt{g_0' h_0}/l_0$. Lines indicate the asymptotes for the inertial and viscous phases: $\tilde{x}_f \sim \tilde{t}^{2/3}$ in (*a*) and $\tilde{u}_f \sim \tilde{t}^{-1/3}$ in (*b*) represent the asymptote in the inertial phase and $\tilde{x}_f \sim \tilde{t}^{3/8}$ (*a*), $\tilde{u}_f \sim \tilde{t}^{-5/8}$ (*b*) (Hoult 1972) and $\tilde{x}_f \sim \tilde{t}^{1/5}$ (*a*), $\tilde{u}_f \sim \tilde{t}^{-4/5}$ (*b*) (Huppert 1982) represent the asymptotes in the viscous phase.

When a gravity current propagates into the deceleration phase on a sufficiently high slope angle, the 'cloud' goes through a distance where the power-relationship applies. Afterwards, the interface of the head is lifted and the uplifted mixed fluid is largely engulfed by the ambient fluid. The heavy fluid contained in the head, i.e. the driving force, is significantly reduced after this process repeats itself a few times. Ultimately, the gravity currents no longer propagate as a 'cloud' entity but as a patch of mixed fluid of low density difference and the patch velocity decays with downslope distance more rapidly. Another plausible route to the finale of a gravity current is for low slope angles. In this case, the gravity current head loses the clear 'cloud' shape in the deceleration phase and tends to spread on the slope without violent mixing with ambient fluid. Gravity currents on low slope angles propagate with the streamlined pattern into the stage of motion when the viscous effects dominate.

In the previous work by Maxworthy (2010), K_M was reported to vary erratically between 2.5 and 2.9 at $\theta = 5.9°, 10.6°$ without clear dependence on the slope angle.

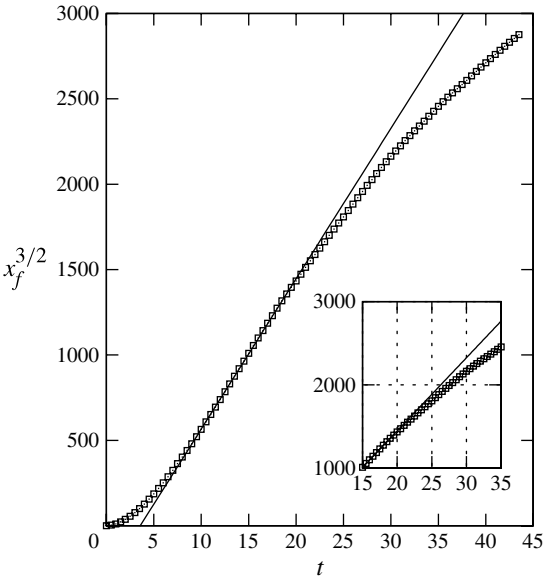

FIGURE 14. Experiment 10/10/12-3: ${x_f}^{3/2}$ versus t for the gravity current produced from $h_0/l_0 = 8$ cm/10 cm and $g_0' = 17.40$ cm s^{-2} on a horizontal boundary. The front location is in units of cm and time is in s. The solid line represents the straight line of best fit to the inertial phase and gives the fitting equation ${x_f}^{3/2} = 88.0(t + t_0)$, where $t_0 = -3.6$ s and the distance to the front is measured from the gate rather than from the virtual origin. In this case the maximum velocity $u_f = 7.46$ cm s^{-1} occurs at $t \approx 4.5$ s and $x_f \approx 29$ cm.

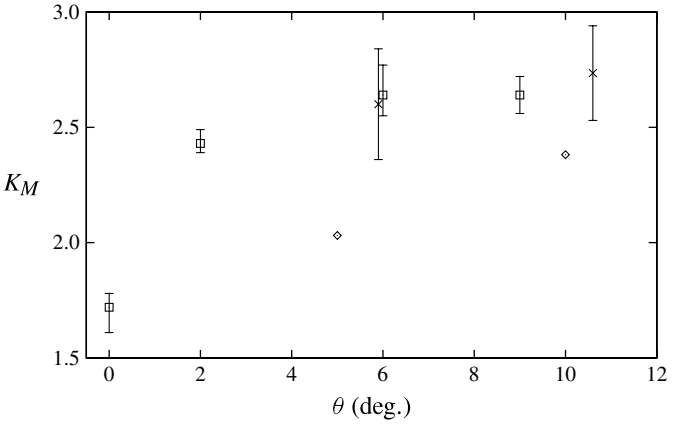

FIGURE 15. Experimental constant K_M versus slope angle θ. Symbols: ⊡, present study; ×, experimental data reported in Maxworthy (2010); ⋄, renormalized from experimental data in Beghin *et al.* (1981) and using (1.8).

Figure 15 shows that our results at $\theta = 6°, 9°$ are consistent with previous reports and it is very likely that in the slope angle range $6° \lesssim \theta \lesssim 10°$, K_M would take its maximum value $K_M \approx 2.64$ without clear dependence on the slope angle. According to our results, K_M would decrease as the slope angle decreases below this range, or as the

slope angle increases beyond this range, which is inferred from the front velocity data in the deceleration phase reported in Beghin *et al.* (1981) and (1.8).

Using the power-relationship, it is possible to estimate the fraction of heavy fluid in the lock that is contained within the head, via $\chi = [K_M/K_B]^3$. The theoretical estimates here are in good agreement with experimental results, but surprisingly those estimates were dramatically low in the previously published work by Maxworthy (2010). For example, it was reported that the maximum buoyancy contained in the head was ∼44 % of the total released buoyancy for a gravity current produced from a buoyancy source of $h_0/l_0 = 10$ cm/10 cm and the ratio was ∼35 % for a gravity current from a source of $h_0/l_0 = 9.7$ cm/5.5 cm, which are both significantly lower than the observations made here. One of the reasons is that the model constant K_B, which is used in the estimation of χ, was incorrect therein, and so was the ratio χ. Here we provide a correct expression for K_B as (1.7) and (A 10) for reference. Another possible reason is that only the core region, e.g. $c \geqslant 0.6$ in figure 6, was deemed to be the head instead, and as such the buoyancy contained within the head region was experimentally underestimated.

One of the limitations in this study is the limited range of slope angle investigated, as has been the case in many previously published works. It is also our hope that further studies for gravity currents on higher slope angles will be continued when a sufficiently deep channel is built.

Acknowledgements

The author wishes to thank Drs B. Maurer, P. Linden and S. Dalziel at the University of Cambridge, S. Balachandar at the University of Florida, M. Garcia and G. Parker at the University of Illinois at Urbana-Champaign for encouragement and helpful discussions at different stages of the work. The author also thanks Mr H. Y. Chou and Mr Y. Y. Chen for their help in running the experiments. Funding support from the National Science Council of Taiwan through grants NSC-98-2218-E-032-007 and NSC-101-2628-E032-003-MY3 is also greatly acknowledged.

Appendix A. Derivation of model constant K_B

In this section, we re-derive the solution to thermal theory, its asymptotic forms, and the model constant K_B in detail.

From (1.3), the height and length of the gravity current head are

$$H = \frac{1}{2}\frac{S_2}{S_1}k^{1/2}\alpha x \quad \text{and} \quad L = \frac{1}{2}\frac{S_2}{S_1}k^{-1/2}\alpha x, \tag{A 1}$$

where x is the distance from the 'virtual origin' to the mass-centre of gravity current head. The 'virtual origin' is located x_0 beyond the lock gate.

Since the front location of gravity current is a more readily measurable quantity, it is desired to rewrite the solution in terms of the front location, x_f. Using the geometric relation $x_f = x + L/2$ and the identity $\alpha = [2S_1/S_2k^{1/2}]\alpha_0$ for the angle of growth α_0, the following relationship, which translates from the mass-centre coordinate system to that using the front location, is derived as

$$x_f = \left(1 + \frac{\alpha_0}{2k}\right)x. \tag{A 2}$$

With Boussinesq approximations and upon substitution of (A 1) into (1.1), the momentum equation becomes

$$U\frac{\mathrm{d}}{\mathrm{d}x}(x^2U) = C - \frac{C_f}{(1+2k)\alpha_0 S_1}(xU^2), \tag{A 3}$$

where

$$C = \frac{4}{\pi}\frac{k}{1+2k}\frac{1}{{\alpha_0}^2}\chi B_0' \sin\theta \quad \text{with } B_0' = \epsilon g A_0, \tag{A 4}$$

is the driving force term. The following closed-form solution is then derived:

$$U^2 = U_0^2\left(\frac{x_0}{x}\right)^{4+2C_f/(1+2k)\alpha_0 S_1} + \frac{2}{3+2C_f/(1+2k)\alpha_0 S_1} \times C\frac{1}{x}\left[1-\left(\frac{x_0}{x}\right)^{3+2C_f/(1+2k)\alpha_0 S_1}\right], \tag{A 5}$$

where U_0 is the initial mass-centre velocity. Transforming (A 3) into the coordinate system using the front location, i.e. $x_f = (1+\alpha_0/2k)x$ and $u_f = (1+\alpha_0/2k)U$, we have

$$u_f^2 = u_{f0}^2\left(\frac{x_{f0}}{x_f}\right)^{4+2C_f/(1+2k)\alpha_0 S_1} + \frac{2}{3+2C_f/(1+2k)\alpha_0 S_1} \times C\left(1+\frac{\alpha_0}{2k}\right)^3\frac{1}{x_f}\left[1-\left(\frac{x_{f0}}{x_f}\right)^{3+2C_f/(1+2k)\alpha_0 S_1}\right], \tag{A 6}$$

where u_{f0} is the initial front velocity, x_{f0} is the distance from the 'virtual origin' to the initial front location and $x_{f0} = (1+\alpha_0/2k)x_0$.

If the gravity current starts from a quiescent initial condition, the solution (A 6) can be further simplified when the gravity current is sufficiently far into the deceleration phase, i.e. when $x_f/x_{f0} \gg 1$,

$$u_f = \left[2/(3+2C_f/(1+2k)\alpha_0 S_1)\right]^{1/2} C^{1/2}(1+\alpha_0/2k)^{3/2}{x_f}^{-1/2}. \tag{A 7}$$

Upon integration, (A 7) can be rewritten in the following form with an integration constant t_0:

$$x_f = K_B{\chi}^{1/3}{B_0'}^{1/3}(t+t_0)^{2/3}, \tag{A 8}$$

where

$$K_B = \left(\frac{9}{6+4C_f/(1+2k)\alpha_0 S_1}\right)^{1/3}\left(\frac{4}{\pi}\right)^{1/3}(1+\alpha_0/2k)[k\sin\theta/\alpha_0^2(1+2k)]^{1/3}. \tag{A 9}$$

When $C_f = 0$, K_B reduces to

$$K_B = \left(\frac{6}{\pi}\right)^{1/3}\left(1+\frac{\alpha_0}{2k}\right)\left[\frac{k\sin\theta}{(1+2k)\alpha_0^2}\right]^{1/3}. \tag{A 10}$$

We should note that $K_M = K_B\chi^{1/3}$ in Maxworthy (2010) and (A 8) can be equivalently written as

$${x_f}^{3/2} = {K_M}^{3/2}{B_0'}^{1/2}(t+t_0). \tag{A 11}$$

If the front location is measured from the lock gate rather than from the virtual origin and x_0 represents the distance from the virtual origin to the lock gate, the front

location x_f should then be replaced by $x_f + x_0$. In this case, the front velocity asymptote and the power-relationship for the front location in the deceleration phase then read

$$u_f = [2/(3 + 2C_f/(1 + 2k)\alpha_0 S_1)]^{1/2} C^{1/2}(1 + \alpha_0/2k)^{3/2}(x_f + x_0)^{-1/2} \tag{A 12}$$

and

$$(x_f + x_0)^{3/2} = {K_M}^{3/2} {B_0'}^{1/2}(t + t_0), \tag{A 13}$$

respectively.

Appendix B. Scaling analysis for the viscous effects

Here we provide a scaling analysis to estimate the front location history when viscous effects become important. The order of magnitude of the forces per unit volume of the gravity current head is estimated as follows.

Gravity:

$$\rho \frac{B_0' \sin\theta}{S_1 HL} \sim \rho \frac{B_0'}{(x_0 + x_f)^2}, \tag{B 1}$$

which indicates that the gravity force per unit volume of the gravity current head reduces as the current propagates. As we understand from the experiments, entrainment of ambient fluid causes the dilution of the moving heavy fluid contained in the head.

Inertia:

$$\rho \frac{(x_0 + x_f)}{t^2}, \tag{B 2}$$

where the acceleration is estimated as $(x_0 + x_f)t^{-2}$ in order of magnitude.

Viscous force:

$$\rho \nu \frac{(x_0 + x_f)}{t} \frac{1}{\delta} \frac{1}{\sqrt{A_0}} \sim \rho \nu^{1/2} \frac{(x_0 + x_f)}{t^{3/2}} \frac{1}{\sqrt{A_0}}, \tag{B 3}$$

where the viscous stress is estimated as $\rho\nu(x_0 + x_f)/t\delta$ and $\sqrt{A_0}$ is an inherent length scale for the 'active' moving head. The thickness of the boundary layer at the edge of the moving head is estimated as $\delta \sim (\nu t)^{1/2}$.

In the early deceleration phase when gravity and inertia forces are important, using (B 1) and (B 2) we derive

$$(x_0 + x_f)^{3/2} \sim {B_0'}^{1/2} t, \tag{B 4}$$

which is consistent with the power-relationship (1.6).

In the late deceleration phase when the front location data deviate from the power-relationship, we propose that a balance between gravity and viscous forces is struck, and using (B 1) and (B 3) we derive

$$(x_0 + x_f)^2 \sim \left(\frac{{B_0'}^2 A_0}{\nu} \right)^{1/3} t, \tag{B 5}$$

which suggests that $(x_0 + x_f)^2 \sim t$ when viscous effects become important.

Figure 16 shows the relationship between $(x_f + x_0)^2$ and t for experiment 10/03/12-1 of the gravity current with $g_0' = 17.11$ cm s^{-2} on a 9° slope. A smooth

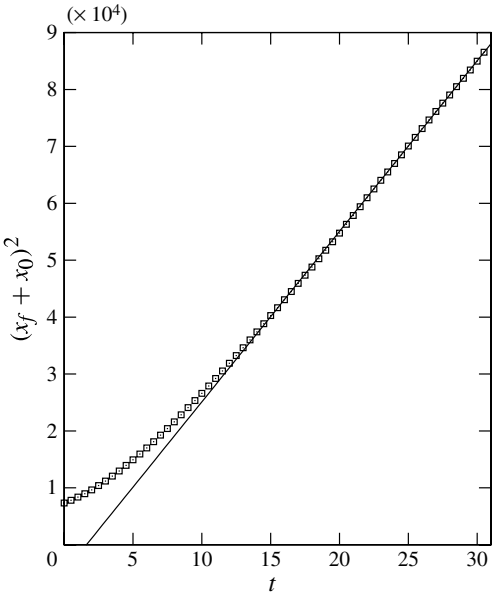

FIGURE 16. Experiment 10/03/12-1: $(x_f + x_0)^2$ versus t for the gravity current with $g_0' = 17.11\ \mathrm{cm\ s^{-2}}$ on a 9° slope. The front location is in units of cm and time is in s. The solid line represents the straight line of best fit to the data at $t \gtrsim 24$ s and the fitting equation is $(x_f + x_0)^2 = 2996.0(t - t_0)$, where $x_0 = 85.6$ cm and $t_0 = 1.6$ s. In this case the maximum front velocity occurs at $t \approx 6.5$ s and the front location data deviate from the power-relationship (1.6) when $t \gtrsim 24$ s.

transition from the inertia-dominated region to the late deceleration phase where viscous effects become important is observed. Good agreement between the front location data and the asymptotic relationship $(x_0 + x_f)^2 \sim t$ in the late deceleration phase indicates that viscous effects could become more important when the front location data deviate from the power-relationship (1.6) in the late deceleration phase.

REFERENCES

ADDUCE, C., SCIORTINO, G. & PROIETTI, S. 2012 Gravity currents produced by lock-exchanges: experiments and simulations with a two layer shallow-water model with entrainment. *J. Hydraul. Engng* **138** (2), 111–121.

BAINES, P. G. 2001 Mixing in flows down gentle slopes into stratified environments. *J. Fluid Mech.* **443**, 237–270.

BAINES, P. G. 2005 Mixing regimes for the flow of dense fluid down slopes into stratified environments. *J. Fluid Mech.* **538**, 245–267.

BATCHELOR, G. K. 1967 *An Introduction to Fluid Dynamics*. Cambridge University Press.

BEGHIN, P., HOPFINGER, E. J. & BRITTER, R. E. 1981 Gravitational convection from instantaneous sources on inclined boundaries. *J. Fluid Mech.* **107**, 407–422.

BIRMAN, V. K., BATTANDIER, B. A., MEIBURG, E. & LINDEN, P. F. 2007 Lock-exchange flows in sloping channels. *J. Fluid Mech.* **577**, 53–77.

BRITTER, R. E. & LINDEN, P. F. 1980 The motion of the front of a gravity current travelling down an incline. *J. Fluid Mech.* **99**, 531–543.

CANTERO, M., LEE, J., BALACHANDAR, S. & GARCIA, M. 2007 On the front velocity of gravity currents. *J. Fluid Mech.* **586**, 1–39.

DADE, W. B., LISTER, J. R. & HUPPERT, H. E. 1994 Fine-sediment deposition from gravity surges on uniform slopes. *J. Sedim. Res.* **64**, 423–432.

DALZIEL, S. B. 2012 *DigiFlow User Guide*. Dalziel Research Partners.

ELLISON, T. H. & TURNER, J. S. 1959 Turbulent entrainment in stratified flows. *J. Fluid Mech.* **6**, 423–448.

FANNELOP, T. K. 1994 *Fluid Mechanics for Industrial Safety and Environmental Protection*. Elsevier.

HOPFINGER, E. J. 1983 Snow avalanche motion and related phenomena. *Annu. Rev. Fluid Mech.* **15**, 47–76.

HOULT, D. P. 1972 Oil spreading on the sea. *Annu. Rev. Fluid Mech.* **4**, 341–368.

HUPPERT, H. 1982 The propagation of two-dimensional and axisymmetric viscous gravity currents over a rigid horizontal boundary surface. *J. Fluid Mech.* **121**, 43–58.

HUPPERT, H. & SIMPSON, J. 1980 The slumping of gravity currents. *J. Fluid Mech.* **99**, 785–799.

LA ROCCA, M., ADDUCE, C., LOMBARDI, V., SCIORTINO, G. & HINKERMANN, R. 2012*a* Development of a lattice Boltzmann method for two-layered shallow-water flow. *Intl J. Numer. Meth. Fluids* **70** (8), 1048–1072.

LA ROCCA, M., ADDUCE, C., SCIORTINO, G., BATEMAN, P. A. & BONIFORTI, M. A. 2012*b* A two-layer shallow water model for 3d gravity currents. *J. Hydraul Res.* **50** (2), 208–217.

LA ROCCA, M., ADDUCE, C., SCIORTINO, G. & PINZON, A. B. 2008 Experimental and numerical simulation of three-dimensional gravity currents on smooth and rough bottom. *Phys. Fluids* **20** (10), 106603.

MARINO, B., THOMAS, L. & LINDEN, P. 2005 The front condition for gravity currents. *J. Fluid Mech.* **536**, 49–78.

MAXWORTHY, T. 2010 Experiments on gravity currents propagating down slopes. Part 2. The evolution of a fixed volume of fluid released from closed locks into a long, open channel. *J. Fluid Mech.* **647**, 27–51.

MAXWORTHY, T. & NOKES, R. I. 2007 Experiments on gravity currents propagating down slopes. Part 1. The release of a fixed volume of heavy fluid from an enclosed lock into an open channel. *J. Fluid Mech.* **584**, 433–453.

MONAGHAN, J. J., CAS, R. A. F., KOS, A. M. & HALLWORTH, M. 1999 Gravity currents descending a ramp in a stratified tank. *J. Fluid Mech.* **379**, 39–69.

NOGUEIRA, H. I. S., ADDUCE, C., ALVES, E. & FRANCA, M. J. 2013 Image analysis technique applied to lock-exchange gravity currents. *Meas. Sci. Technol.* **24**, 047001.

RASTELLO, M. & HOPFINGER, E. J. 2004 Sediment-entraining suspension clouds: a model of powder-snow avalanches. *J. Fluid Mech.* **509**, 181–206.

ROSS, A. N., LINDEN, P. F. & DALZIEL, S. B. 2002 A study of three-dimensional gravity currents on a uniform slope. *J. Fluid Mech.* **453**, 239–261.

SEON, T., ZNAIEN, J., PERRIN, B., HINCH, E. J., SALIN, D. & HULIN, J. P. 2007 Front dynamics and macroscopic diffusion in buoyant mixing in tilted tubes. *Phys. Fluids* **19**, 125105.

SHIN, J., DALZIEL, S. & LINDEN, P. 2004 Gravity currents produced by lock exchange. *J. Fluid Mech.* **521**, 1–34.

SIMPSON, J. 1997 *Gravity Currents*, 2nd edn. Cambridge University Press.

TICKLE, G. 1996 A model of the motion and dilution of a heavy gas cloud released on a uniform slope in calm conditions. *J. Hazard. Mater.* **49**, 29–47.

WEBBER, D., JONES, S. & MARTIN, D. 1993 A model of the motion of a heavy gas cloud released on a uniform slope. *J. Hazard. Mater.* **33**, 101–122.